Supporting Information for "*Ab Initio* Force Fields for Imidazolium-Based Ionic Liquids."

Jesse G. McDaniel,[†] Eunsong Choi,[‡] Chang Yun Son,[†] J. R. Schmidt,[†] and Arun Yethiraj[*,†]

Department of Chemistry, University of Wisconsin, Madison, Wisconsin, 53706, and Department of Physics,University of Wisconsin, Madison, Wisconsin, 53706

E-mail: yethiraj@chem.wisc.edu

[*]To whom correspondence should be addressed
[†]Department of Chemistry, University of Wisconsin, Madison, Wisconsin, 53706
[‡]Department of Physics,University of Wisconsin, Madison, Wisconsin, 53706

S1 Force Field Parameters

In Table S1, we give a comprehensive list of parameters used to describe the non-bonded interactions in all of the ionic liquids studied in this work. We note that for the exponential repulsive terms, the coefficients A_{ij}^{tot} result from a sum of like atom-type coefficients describing exchange, electrostatic, induction, and dhf interactions (see reference).

$A_{ij}^{tot} = A_{ij}^{exch} + A_{ij}^{elec} + A_{ij}^{ind} + A_{ij}^{dhf}$

All cross-interactions are treated using the following combination rules:

$|A_{ij}^{type}| = (A_i^{type} A_j^{type})^{1/2}$

$$B_{ij} = (B_i + B_j)\frac{B_i B_j}{B_i^2 + B_j^2}$$

$$C_n^{ij} = \sqrt{C_n^i C_n^j}$$

Where the sign of A_{ij}^{type} is strictly positive for exchange, and strictly negative for electrostatics, induction, and dhf.

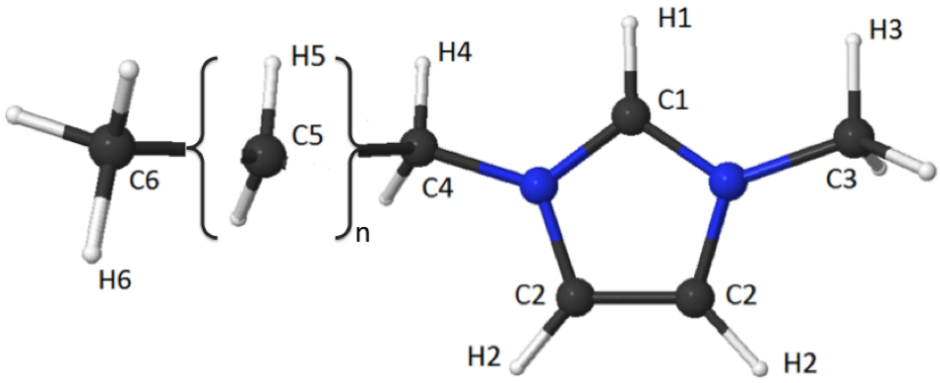

Figure S1: Atom labels for $EMIM^+$, $BMIM^+$, and C_6MIM^+, where the number of C5 carbon atoms is n=0, n=2, and n=4 respectively.

S1.1 Non-Bonded Parameters

Table S1: Non-bonded force field parameters. Atom types are depicted in Figure S1. Units are as follows: A_{exch}, A_{elec}, A_{ind}, and A_{dhf} are in kJ/mol; B are in Å^{-1}; C_6 are in kJ/(mol·Å^{-6}), C_8 are in kJ/(mol·Å^{-8}), C_{10} are in kJ/(mol·Å^{-10}), C_{12} are in kJ/(mol·Å^{-12}), polarizabilities (α) are in Å^3.

Atom type	A_{exch}	A_{elec}	A_{ind}	A_{dhf}	B
N	252624.4	102233.5	0.0	17537.3	3.9061
C1	422654.8	198880.5	0.0	39863.4	3.4384
C2	422654.8	198880.5	0.0	39863.4	3.4384
C3	304938.7	117598.0	11.7	2837.1	3.4384
C4	304938.7	117598.0	11.7	2837.1	3.4384
C5	304938.7	117598.0	11.7	2837.1	3.4384
C6	304938.7	117598.0	11.7	2837.1	3.4384
H1	5241.8	305.2	0.0	540.4	3.7776
H2	5241.8	305.2	0.0	540.4	3.7776
H3	15986.7	3623.5	746.7	1467.9	3.7776
H4	15986.7	3623.5	746.7	1467.9	3.7776
H5	15986.7	3623.5	746.7	1467.9	3.7776
H6	15986.7	3623.5	746.7	1467.9	3.7776
B	11862.8	0.0	0.0	0.0	2.9518
P	0.0	0.0	0.0	0.0	3.3184
F	180128.4	80998.3	0.0	13995.8	3.5961

Atom type	C_6	C_8	C_{10}	C_{12}	α
N	1018.7	6246.0	92197.5	676941.7	1.047
C1	1414.9	6158.8	94108.3	505703.4	1.953
C2	1414.9	6158.8	94108.3	505703.4	1.953
C3	716.6	0.0	0.0	0.0	1.953
C4	716.6	0.0	0.0	0.0	1.953
C5	1354.5	5705.0	18089.8	52097.7	1.953
C6	1354.5	5705.0	18089.8	52097.7	1.953
H1	49.4	125.1	2245.6	0.0	0.000
H2	49.4	125.1	2245.6	0.0	0.000
H3	129.4	679.6	4995.3	0.0	0.000
H4	129.4	679.6	4995.3	0.0	0.000
H5	129.4	679.6	4995.3	0.0	0.000
H6	129.4	679.6	4995.3	0.0	0.000
B	973.3	5319.1	53711.0	330184.6	0.035
P	3582.1	30062.5	118008.9	0.0	0.555
F	795.3	5754.0	27552.6	85759.4	0.932

S1.2 Charges

Table S2: Cation charges; atom types are depicted in Figure S1.

Atom type	$EMIM^+$	$BMIM^+$	C_6MIM^+
N	-0.1965	-0.1915	-0.2046
C1	0.3197	0.3158	0.3142
C2	-0.0167	-0.0192	-0.0186
C3	0.2481	0.2316	0.2725
C4	0.3189	0.2341	0.3179
C5	N/A	0.0616	0.0651
C6	-0.3067	-0.0251	0.0404
H1	0.0922	0.0919	0.0921
H2	0.1635	0.1644	0.1637
H3	0.0291	0.0328	0.0222
H4	0.0096	0.0157	-0.0106
H5	N/A	-0.0181	-0.0264
H6	0.1069	0.0213	-0.0043

Table S3: BF_4^- charges.

Atom type	q
B	1.2008
F	-0.5502

Table S4: PF_6^- charges

Atom type	q
P	1.7624
F	-0.4604

S1.3 Proper Dihedrals

Given in the tables below are the Ryckaert-Belleman parameters (in kJ/mol) describing the proper dihedral potentials for the cation alkyl chains, that were explicitly fit to ab initio calculations. Note as stated in the paper, all alkyl-chain dihedral potentials involving hydrogen atoms are assumed zero, unless explicitly listed otherwise (terminal group).

Table S5: EMIM$^+$proper dihedrals

Dihedral type	C_0	C_1	C_2	C_3	C_4	C_5
C1-N-C4-C6	0.000	-0.105	-0.114	1.906	-6.345	3.933
C2-N-C4-C6	0.000	0.105	-0.114	-1.906	-6.345	-3.933
N-C4-C6-H6	0.000	18.447	19.558	-7.641	-4.946	0.012

Table S6: BMIM$^+$proper dihedrals

Dihedral type	C_0	C_1	C_2	C_3	C_4	C_5
C1-N-C4-C5	0.000	-2.438	1.111	3.314	-1.146	0.098
C2-N-C4-C5	0.000	2.438	1.111	-3.314	-1.146	-0.098
N-C4-C5-C5	0.000	15.411	0.638	-21.200	1.871	-0.704
C4-C5-C5-C6	0.000	17.570	-3.260	-18.734	1.725	-1.516
C5-C5-C6-H6	0.000	16.880	-4.247	-5.037	2.274	-3.638

Table S7: C_6MIM$^+$proper dihedrals

Dihedral type	C_0	C_1	C_2	C_3	C_4	C_5
C1-N-C4-C5	0.000	-1.516	-0.028	1.405	-0.377	0.413
C2-N-C4-C5	0.000	1.516	-0.028	-1.405	-0.377	-0.413
N-C4-C5-C5	0.000	16.518	0.599	-24.09	1.951	0.111
C4-C5-C5-C5	0.000	15.819	-3.537	-18.67	1.656	-1.598
C5-C5-C5-C5	0.000	16.118	-2.326	-20.13	1.166	-0.816
C5-C5-C5-C6	0.000	17.709	0.502	-24.05	0.450	-0.848
C5-C5-C6-H6	0.000	10.933	2.145	-7.954	-1.026	1.074

S2 Force Field Fits

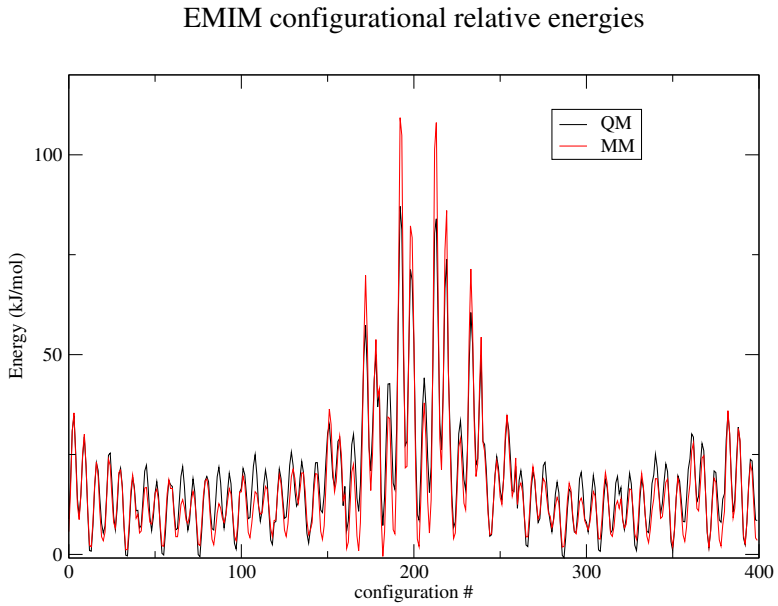

Figure S2: Force field vs ab initio relative energies for configurations sampling different $EMIM^{+}$dihedral distributions

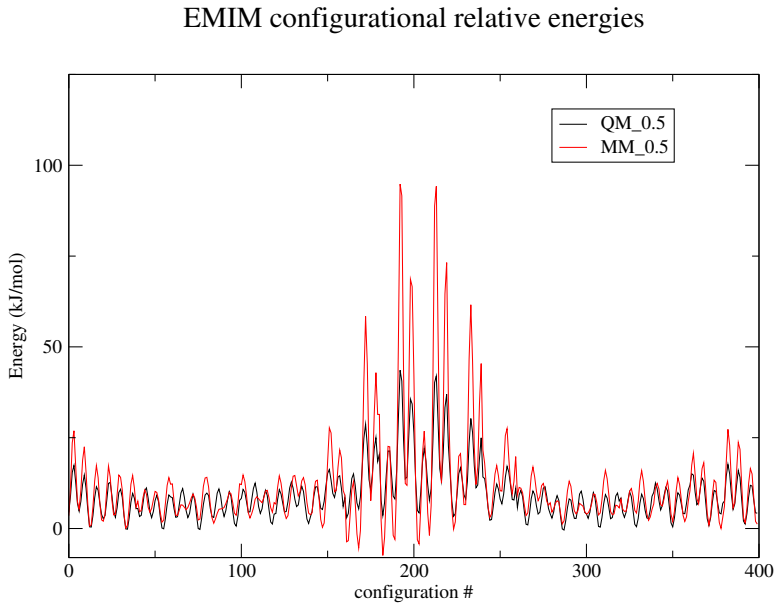

Figure S3: Analogous fit to Figure S2 for the ab initio PES scaled by 0.5

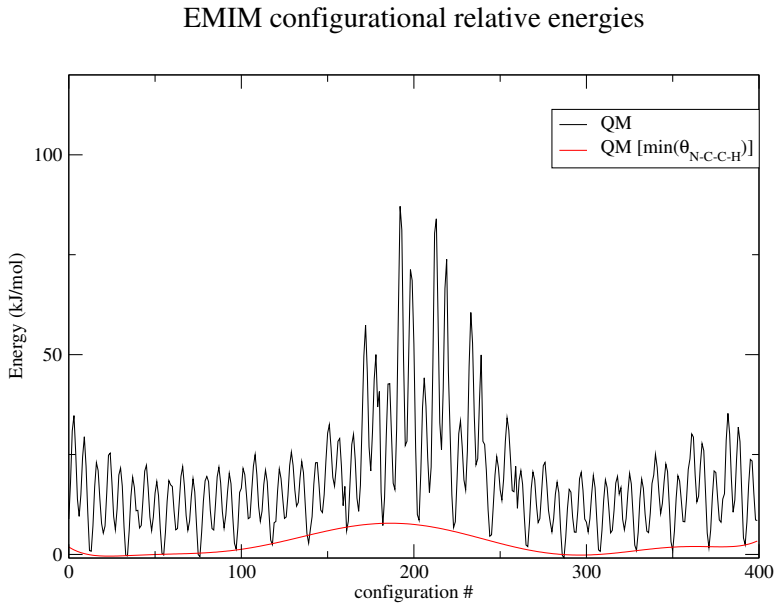

Figure S4: EMIM PES given by $E(\theta_{C-N-C-C}) = min_{\theta_{N-C-C-H}} E(\theta_{C-N-C-C}, \theta_{N-C-C-H})$ (red), compared to original *ab initio* surface.

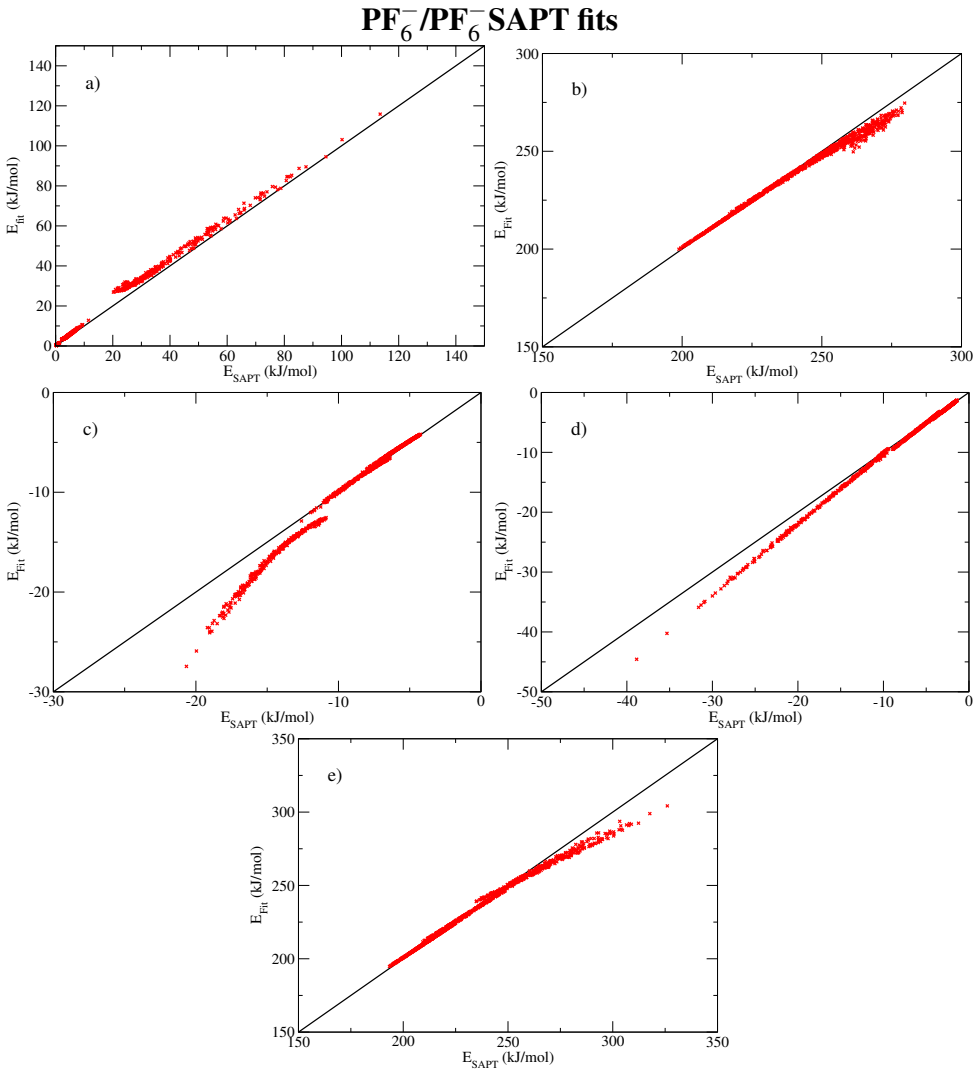

Figure S5: PF_6^-/PF_6^- SAPT intermolecular interaction fits: a) exchange, b) electrostatics, c) induction+dhf, d) dispersion, e) total energy.

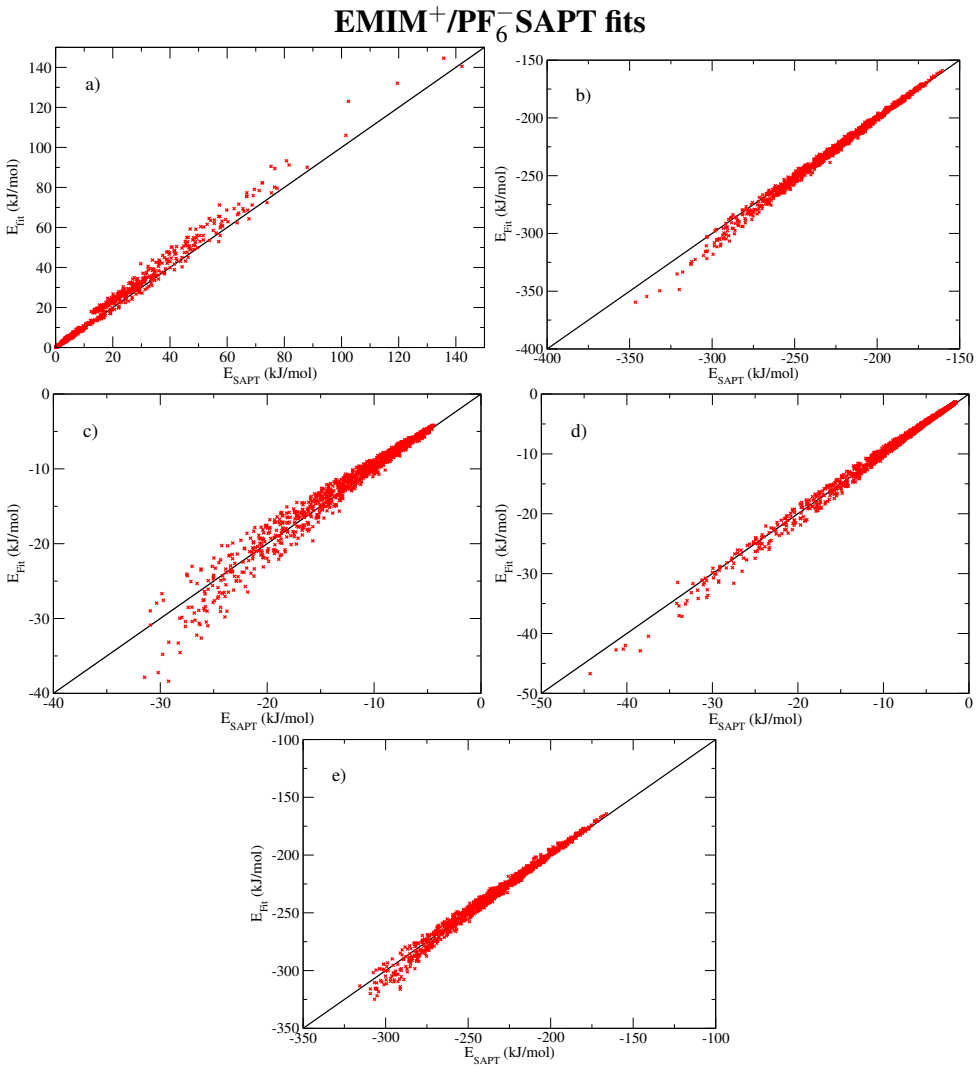

Figure S6: $EMIM^+/PF_6^-$ SAPT intermolecular interaction fits: a) exchange, b) electrostatics, c) induction+dhf, d) dispersion, e) total energy.

S3 Section 3: Thermodynamic properties

S3.1 System Equilibration

For our MD simulations, we have used a comparatively short simulation time for equilibration in the NPT ensemble (2 ns) compared to the production runs in the NVT ensemble (50 ns). This partitioning of computational effort was chosen for maximal statistics. Here, we demonstrate the sufficiency of the employed equilibration time for the most viscous IL studied, $[C_6MIM^+][PF_6^-]$,

at the lowest temperature, 298 K; all other simulations for different IL/temperature combinations should equilibrate as least as fast. Figure S7(a) shows the density of $[C_6MIM^+][PF_6^-]$at 298 K as a function of time for the NPT equilibration simulation. It is clear that the density reaches its equilibrium value extremely rapidly (in the first 100 ps), and subsequently fluctuates about this value. In Figure S7(b), we show various energy components for $[C_6MIM^+][PF_6^-]$at 298 K over the 50 ns of the NVT simulation. We do not elaborate on the nature of the decomposition, but it is clear that these distinct energy components as well as the total potential energy of the system do not change over the course of the simulation, indicating that the system was indeed sufficiently equilibrated.

We note that currently employed equilibration times may not be sufficient for ILs composed of longer alkyl-chain cations, such as C_8MIM^+. For such ILs, there exists significant structural heterogeneity involving partitioning into polar and non-polar domains; accurately reproducing this heterogeneity may require longer equilibration times. However, for $C_6MIM^+$and shorter-chain cations, the structural heterogeneity is much less significant (see for example, Triolo et al. *J. Phys. Chem. B* **2007**, 111, 4641-4644), rendering more rapid equilibration.

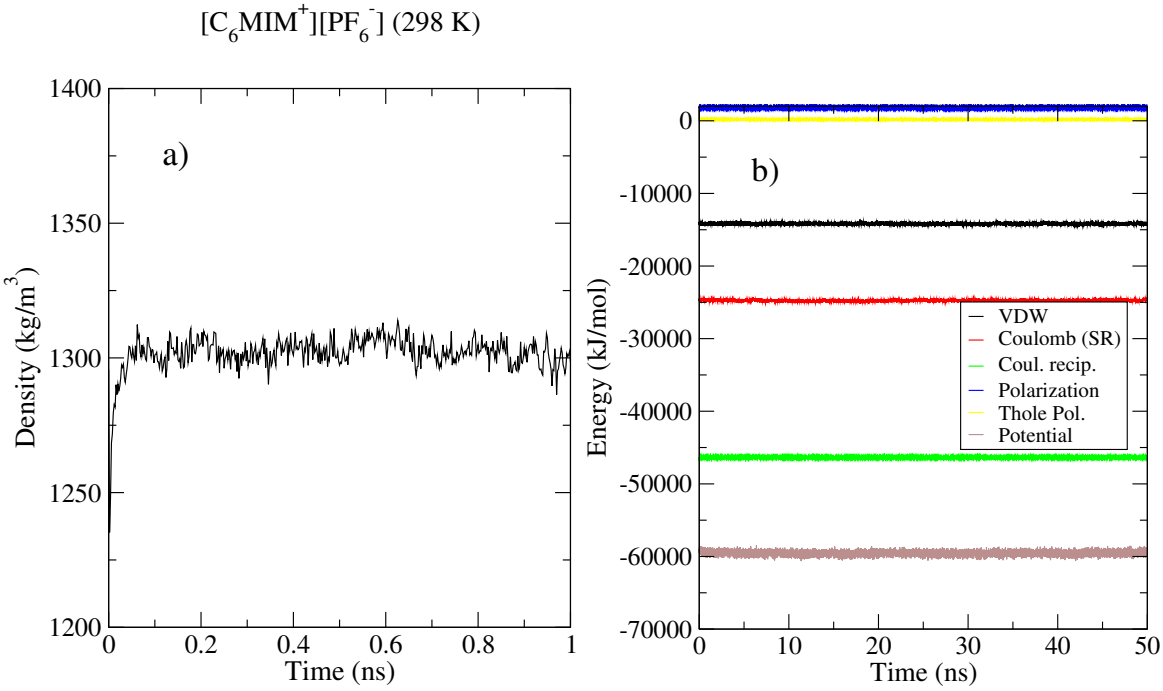

Figure S7: a) Density of $[C_6MIM^+][PF_6^-]$at 298K for initial 1 ns of NPT simulation. b) Energy components of $[C_6MIM^+][PF_6^-]$at 298K for 50 ns NVT simulation.

S3.2 $[EMIM^+][BF_4^-]$Dihedral Distributions

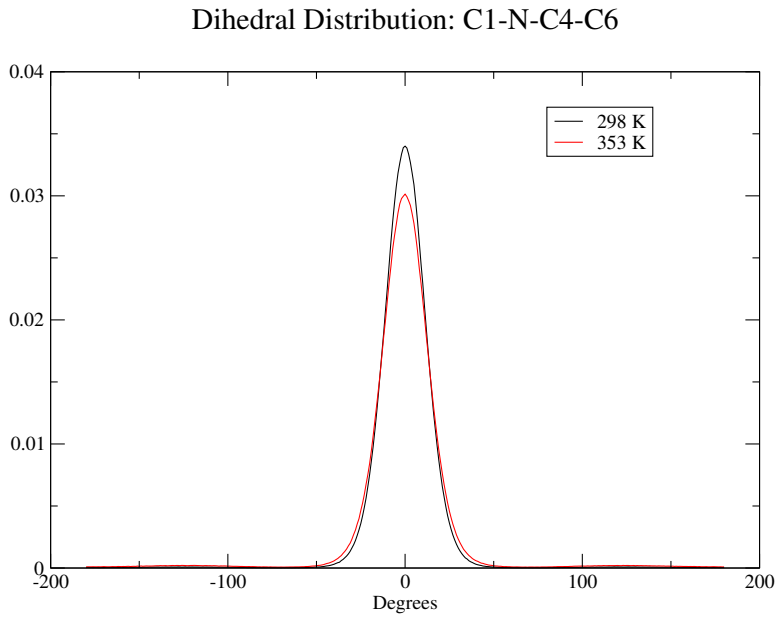

Figure S8: EMIM dihedral distribution for ab initio surface of Figure S2 for [EMIM$^+$][BF$_4^-$].

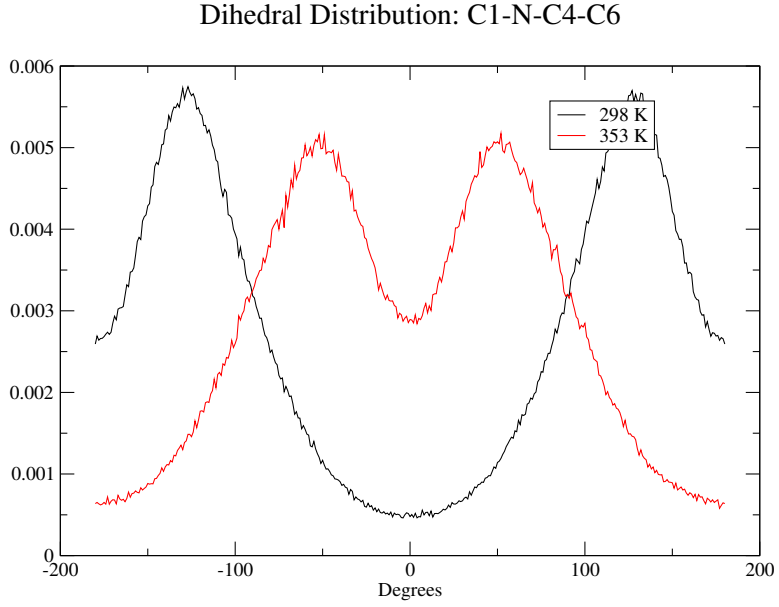

Figure S9: EMIM dihedral distribution for smoothed methyl rotation surface of Figure S4 for [EMIM$^+$][BF$_4^-$].

S3.3 Liquid Energies

The total potential energy of the IL liquids at 298 K and 353 K are given in Table S8 (these energies are normalized by the number of ion pairs in the liquid). The uncertainty in these values is < 1 kJ/mol, as determined from comparison of the 10 different [$BMIM^+$][BF_4^-]trajectories at 298 K. We note that these energies are not physically significant, as they include intramolecular contributions. Rather the physically significant quantity is the cohesive energy, which subtracts out the individual ion energies (Table S10), as given in the main paper.

Table S8: Total potential energy of IL liquids, per ion pair. The uncertainty of this data is < 1 kJ/mol. [a] [$EMIM^+$][PF_6^-]is a solid at room temperature.

	Energy kJ/mol	
IL	298 K	353 K
[$EMIM^+$][BF_4^-]	-310	-291
[$EMIM^+$][PF_6^-]	N/A[a]	-275
[$BMIM^+$][BF_4^-]	-310	-288
[$BMIM^+$][PF_6^-]	-294	-270
[C_6MIM^+][BF_4^-]	-312	-286
[C_6MIM^+][PF_6^-]	-298	-270

S3.4 Ion Pair Energies

Gas-phase, ion pair energetics were computed from 200 ns NVT simulations of single ion pairs in a $\sim$ 5 nm box, using a 2 nm cutoff for both electrostatic and VDWs interactions. This cutoff is long enough to ensure all pairwise interactions within the ion pair are included, but short enough to avoid interactions between ion images. We remove both translational and rotational center of mass motion of the system. It is important to ensure equipartition of thermal energy, which is not guaranteed as there are few collisions in the gas phase. To achieve this, we use multiple thermostats for the cation degrees of freedom, implemented with the "temperature group" concept in GROMACS in which the user defines separate groups for independent temperature coupling. We find that defining groups based on atom types, e.g. for cations N1 C1 H1 C3 H3 C5, gives sufficient equipartition of energy (for example, we found poor equipartition of energy for C_6MIM^+using

only a single temperature group). Based on multiple simulation trajectories, we estimate the uncertainties of this data to be $\sim$ 2-3 kJ/mol.

Table S9: Total potential energy of gas-phase ion pair subject to temperature thermostat. The uncertainty of this data is $\sim$ 2-3 kJ/mol.

	Energy kJ/mol	
Ionpair	298 K	353 K
$[EMIM^+][BF_4^-]$	-191	-177
$[EMIM^+][PF_6^-]$	-162	-147
$[BMIM^+][BF_4^-]$	-187	-171
$[BMIM^+][PF_6^-]$	-163	-144
$[C_6MIM^+][BF_4^-]$	-183	-163
$[C_6MIM^+][PF_6^-]$	-163	-142

S3.5 Single Ion Energies

To compute the cohesive energy of the IL liquids, we use isolated single ions as the reference state. We compute the energies of these isolated ions at 298 K and 353 K, running a short (2 ns) simulation of the single ion, subject to a thermostat (again using separate temperature groups for different atom types, see Section S3.4) . We note that the major contribution to the cation energy are the intramolecular electrostatic interactions between atoms separated by three bonds or more (closer atom pairs are excluded). This is the reason why the intramolecular potential energy decreases as the alkyl chain of the cation gets longer, $EMIM^+ > BMIM^+ > C_6MIM^+$. For the larger alkyl chain cations, the unit ion charge is slightly more spread out, reducing the intramolecular electrostatic repulsion. The bond and angle contributions to the energy do increase with increasing alkyl chain length, but this is outweighed by the electrostatic effect.

Table S10: Total intramolecular potential energy of isolated ion subject to temperature thermostat

Ion	Energy kJ/mol	
	298 K	353 K
$EMIM^+$	167	179
$BMIM^+$	163	175
C_6MIM^+	156	168
BF_4^-	14	18
PF_6^-	20	25

S3.6 Diffusion Coefficients

Figure S10 shows the diffusion coefficients as a function of system density for $[BMIM^+][BF_4^-]$at 298 K computed from the 10 different 50 ns trajectories (including the 1600 ion pair simulation). The densities are slightly different for all the systems due to the fact that the independent trajectories were started from different snapshots of the initial NPT equilibration simulation; there is ~ 1 % maximum variation in the system density. This plot suggests that some of the deviation in computed diffusion coefficients, at least the largest outliers, may be explained by density differences (albeit small).

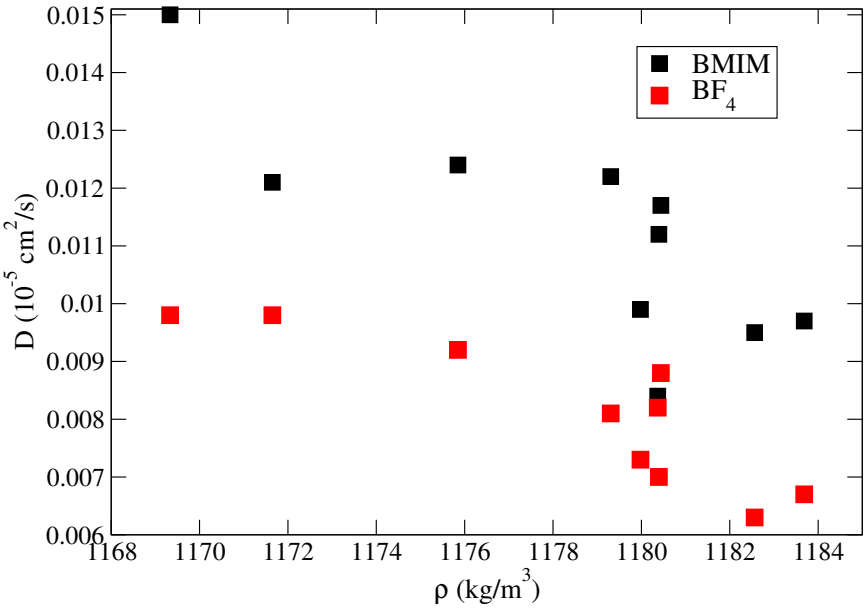

Figure S10: Diffusion coefficients for $[BMIM^+][BF_4^-]$at 298 K as computed from the 10 different trajectories, plotted as a function of the density of the system.